

Electrochemical Behavior of Dy(III) and Formation of Dy-Zn Alloy by Co-Reduction with Zn(II) in Eutectic NaCl-KCl Melts

Zhu, Zengli; Wu, Xiaobin; Hua, Zhongsheng; Xu, Liang; He, Shiwei; Geng, Ao; Yang, Yongxiang; Zhao, Zhuo

DOI

[10.1149/1945-7111/abb27e](https://doi.org/10.1149/1945-7111/abb27e)

Publication date

2020

Document Version

Final published version

Published in

Journal of the Electrochemical Society

Citation (APA)

Zhu, Z., Wu, X., Hua, Z., Xu, L., He, S., Geng, A., Yang, Y., & Zhao, Z. (2020). Electrochemical Behavior of Dy(III) and Formation of Dy-Zn Alloy by Co-Reduction with Zn(II) in Eutectic NaCl-KCl Melts. *Journal of the Electrochemical Society*, 167(12), Article 122509. <https://doi.org/10.1149/1945-7111/abb27e>

Important note

To cite this publication, please use the final published version (if applicable).
Please check the document version above.

Copyright

Other than for strictly personal use, it is not permitted to download, forward or distribute the text or part of it, without the consent of the author(s) and/or copyright holder(s), unless the work is under an open content license such as Creative Commons.

Takedown policy

Please contact us and provide details if you believe this document breaches copyrights.
We will remove access to the work immediately and investigate your claim.

Electrochemical Behavior of Dy(III) and Formation of Dy-Zn Alloy by Co-Reduction with Zn(II) in Eutectic NaCl-KCl Melts

To cite this article: Zengli Zhu *et al* 2020 *J. Electrochem. Soc.* **167** 122509

View the [article online](#) for updates and enhancements.

INTERNATIONAL OPEN ACCESS WEEK
OCTOBER 19-26, 2020

ALL ECS ARTICLES. ALL FREE. ALL WEEK.
www.ecsdl.org

**NOW
AVAILABLE**



Electrochemical Behavior of Dy(III) and Formation of Dy-Zn Alloy by Co-Reduction with Zn(II) in Eutectic NaCl-KCl Melts

Zengli Zhu,¹ Xiaobin Wu,¹ Zhongsheng Hua,^{1,2,z} Liang Xu,^{1,2} Shiwei He,¹ Ao Geng,¹ Yongxiang Yang,^{1,3} and Zhuo Zhao^{1,2,z}

¹School of Metallurgical Engineering, Anhui University of Technology, Ma'anshan 243032, People's Republic of China

²Key Laboratory of Metallurgical Emission Reduction & Resources Recycling, Anhui University of Technology, Ministry of Education, Ma'anshan 243002, People's Republic of China

³Department of Materials Science and Engineering, Delft University of Technology, 2628 CD Delft, The Netherlands

The electrochemical behavior of Dy(III) and its co-reduction process with Zn(II) on a tungsten electrode were studied in eutectic NaCl-KCl melts at 700 °C by using a series of electrochemical techniques. The results indicate that the reduction of Dy(III) to Dy(0) is a diffusion controlled quasi-reversible process through a one-step reaction of exchanging three electrons. The diffusion coefficient of Dy(III) was calculated to be $1.7 \times 10^{-5} \text{ cm}^2 \text{ s}^{-1}$. Furthermore, the co-reduction of Dy(III) and Zn(II) on the tungsten electrode makes Dy(III) be reduced at more positive potentials due to the formation of various Dy-Zn intermetallic compounds. The electromotive force measurements were performed to determine the thermodynamic properties of the Dy-Zn intermetallic compounds, including the activities and relative partial molar Gibbs free energies of dysprosium in the two-phase coexisting state, as well as the standard formation Gibbs energies of Dy-Zn intermetallic compounds. Finally, potentiostatic electrolysis at -2.0 V was carried out in molten NaCl-KCl-DyCl₃ (1.0 mol%)-ZnCl₂ (1.0 mol%) at 700 °C for 11 h to prepare Dy-Zn alloy. X-ray diffraction and scan electron micrograph—energy dispersive spectrometry analyses showed that the obtained Dy-Zn alloy mainly comprised of DyZn₂, as well as the minor phases of Dy₂Zn₁₇, DyZn₃ and DyZn.

© 2020 The Electrochemical Society ("ECS"). Published on behalf of ECS by IOP Publishing Limited. [DOI: [10.1149/1945-7111/abb27e](https://doi.org/10.1149/1945-7111/abb27e)]

Manuscript submitted July 15, 2020; revised manuscript received August 10, 2020. Published September 2, 2020.

To realize waste minimization and fuel reclamation, the processing of nuclear wastes in which radiotoxic but very valuable elements of uranium, plutonium and other minor actinides are contained, has attracted increasing attentions in the countries using nuclear energy.¹ Partitioning and transmutation (P&T), is commonly considered as one of the promising methods to safely dispose spent nuclear fuel, and now has become an important issue for the sustainable development of nuclear energy technologies.²⁻⁴ Generally, most of the uranium and plutonium in spent fuel can be recovered and thus reused in new fuels. The lanthanides, accounting for 25% in weight of the fission products, should be separated from the actinides, because the large neutron absorption cross section would significantly decrease transmutation efficiency of actinides.^{5,6} However, it is extremely challenging to efficiently separate lanthanides from actinides due to their similar physicochemical properties.⁷

The conventional hydrometallurgical process is not effective for lanthanides and actinides extraction for further recycling because of their limited solubilities in aqueous media.⁸ Molten chlorides or fluorides have the multiple attributes of high dissolution of fuel components, low neutron cross section, and high radiation stability and thermal resistance,⁹ and thus the pyrochemical process based on molten salt electrorefining has been regarded as a potential approach for the recovery of actinides (especially transuranium elements) separated from lanthanides.¹⁰ During this process, the spent metallic fuel after pretreatment serving as an anode is electrochemically dissolved into molten salts, and then the uranium is selectively deposited onto a solid cathode owing to the difference in the formation energies, whereas plutonium and minor actinides are gathered into a liquid cathode, usually Bi or Cd, by electrorefining.^{11,12} However, a quantity of lanthanides also get deposited with minor actinides (Np, Am and Cm) because of their extremely similar electrochemical behaviors and low activity coefficients in liquid metal.¹³ Therefore, highly efficient separation from lanthanides is generally required to recover the minor actinides with an acceptable chemical purity.¹⁴

Alloy formation is an effective means for the separation of minor actinides from lanthanides. Both of these two categories of elements are well known to readily form alloys with nobler elements such as

Bi, Cd and Al.^{2,13,15} The deposition of these elements generating an alloy proceeds sensibly toward more positive potentials, and the deposition potential disparity between actinides and lanthanides is more evident. Consequently, the separation of minor actinides from lanthanides could become easier. It was reported that the strong interactions generated between actinides and liquid Al due to the formation of An-Al alloys result in an excellent separation and recovery of minor actinides.^{2,16,17} Contrary to the liquid bismuth or cadmium cathode, Malmbeck et al. found that using solid aluminum cathode facilitates a more efficient separation of actinides while lanthanides remain in the melts.^{18,19} As the electrorefining separation progresses, the lanthanides accumulate in the melts and should be extracted when the concentration increases to 10wt% to regenerate the melts and to avoid reducing the separation efficiency of actinides/lanthanides.^{20,21} In this regard, the investigations on the electrochemical behavior and extraction of lanthanides are of great importance for systematical understanding of the pyrochemical electrorefining process and the efficient utilization of the valuable actinides from spent nuclear fuel.

Dysprosium is a heavy rare earth element in the fission products.²² Although many researches have been conducted to explore the electrochemical behavior of Dy(III) ions in molten salt media, the reduction mechanism of Dy(III) has not yet been fully clarified and is still controversial according to current literature reports. It is reported that the reduction of Dy(III) to Dy metal on inert electrodes in molten LiCl-KCl is a single step process with three electrons exchanged²³⁻²⁶: $\text{Dy(III)} + 3\text{e}^- \leftrightarrow \text{Dy(0)}$. Similarly, Kushkhov et al.²⁷ found that, in NaCl-KCl melts, Dy(III) was also directly reduced to Dy metal on a tungsten electrode through this three-electron transfer process. Moreover, this one-step reduction process of Dy(III) to Dy(0) on an inert electrode has also been observed in molten LiF-CaF₂ by Saïla et al. and Shi et al.^{28,29} On the contrary, Castrillejo et al.³⁰ reported that the electrochemical reduction of Dy(III) on a tungsten electrode in molten LiCl-KCl at 723 K took place in two consecutive steps: $\text{Dy(III)} + \text{e}^- \leftrightarrow \text{Dy(II)}$ and $\text{Dy(II)} + 2\text{e}^- \leftrightarrow \text{Dy(0)}$. However, an earlier study of Liu et al.³¹ proposed that electrochemical reduction of Dy(III) on an inert platinum electrode in NaF-CaF₂ melts at 940 °C consisted of the two consecutive steps involving the intermediate oxidation state of Dy(I). The discrepancy in redox mechanism of dysprosium is probably attributed to the complexity of its electrochemistry in molten salts and the impurity of measurement conditions.

^zE-mail: huazs83@163.com; zhaozhuo1018@163.com

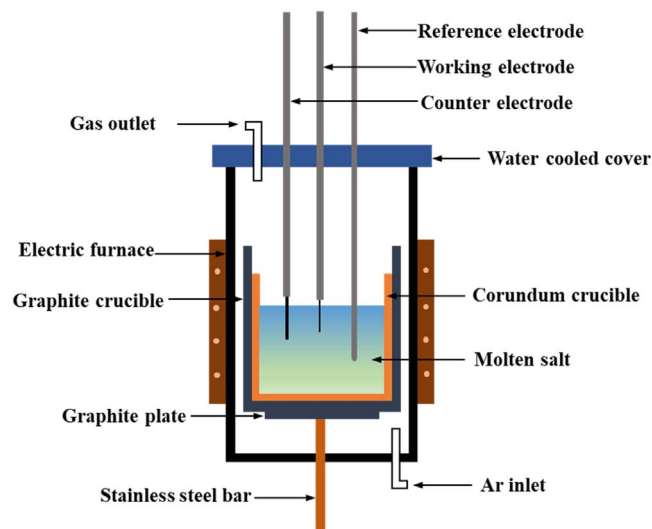


Figure 1. Schematic diagram of the experimental set-up for electrochemical experiments.

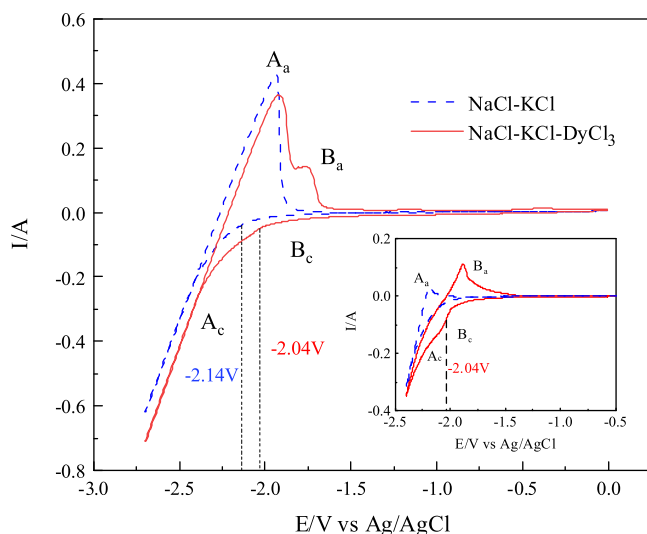


Figure 2. CVs measured on a tungsten electrode ($S = 0.322 \text{ cm}^2$) before (blue dotted line) and after (red solid line) the addition of 1.0 mol% DyCl_3 in NaCl-KCl eutectic melts with different terminal potentials. Temperature: $700 \text{ }^\circ\text{C}$, Scan rate: 0.1 V s^{-1} .

Currently, the dysprosium is usually extracted from molten salts in the form of alloys by electroreduction of Dy(III) on reactive electrodes^{24,32–36} such as Mg, Ni, Fe, Cu and Al. However, reports on extraction of dysprosium via electrochemical deposition with a nobler metal of zinc are fairly limited in open literature. Hence, co-reduction of Dy(III) and Zn(II) yielding Dy-Zn alloy is attempted to facilitate the separation or extraction of dysprosium. The present work is dedicated to reassess the electrochemical behavior of Dy(III) in eutectic NaCl-KCl on a tungsten electrode. In particular, the co-reduction mechanism of Dy(III) and Zn(II) and the thermodynamic properties of Dy-Zn intermetallic compounds are investigated to verify the feasibility of dysprosium extraction by electrochemical deposition with noble metal, and ultimately to propose an efficacious approach for separation of dysprosium from spent nuclear fuel.

Experimental

Preparation of electrolyte melts.—A mixture of anhydrous NaCl and KCl with eutectic composition (50.6:49.4 mol%) was selected as the supporting electrolyte because of the excellent physicochemical

properties and comparatively low cost.^{37,38} The analytical reagents NaCl (>99.5% purity) and KCl (>99.5% purity) were first dried at $200 \text{ }^\circ\text{C}$ for more than 48 h to remove residual moisture, and then melted in a corundum crucible at $700 \text{ }^\circ\text{C}$ in an electric furnace. The temperature of the experiments was determined by a K-type thermocouple. Metal ions impurities in the melts were removed by pre-electrolysis at -2.10 V (vs Ag/AgCl) for 60 min. Anhydrous DyCl_3 (99.6%) and ZnCl_2 (99.95%) powders were directly introduced into the melts as the source of Dy(III) and Zn(II) ions, respectively. All the experiments were performed in a high purity Ar atmosphere to avoid exposure to O_2 and H_2O .

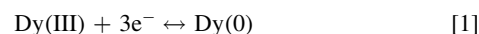
Electrochemical apparatus and electrodes.—The experimental setup used for electrochemical measurements and electrolysis in this work is shown in Fig. 1. All electrochemical measurements including cyclic voltammetry, square wave voltammetry, open circuit chronopotentiometry and potentiostatic electrolysis, were conducted in a three-electrode cell using PARSTAT 2273 electrochemical workstation (Ametek Group Co., American) controlled with the PowerSuite software package. A tungsten wire (99.99% purity) of 1.0 mm in diameter was polished and cleaned thoroughly and thus served as the working electrode. A spectral pure graphite rod (6.0 mm in diameter) was adopted as the counter electrode. The reference electrode was a silver wire (99.99% purity) of 1.0 mm in diameter which is immersed in the molten mixture of NaCl-KCl-AgCl (2.0 mol%) contained in a mullite tube. All the potentials in this study were referred to this Ag^+/Ag couple. The surface area of the working electrode was determined by measuring its immersion depth in the melts.

Preparation and characterization of Dy-Zn alloy.—Dy-Zn alloy was prepared on a tungsten electrode by potentiostatic electrolysis in NaCl-KCl-DyCl₃-ZnCl₂ melts at $700 \text{ }^\circ\text{C}$. After electrolysis, the cathodic deposit was initially washed in distilled water to remove the attached salts and then ultrasonically cleaned with ethanol (>99.5% purity). The phase composition of the alloy samples was identified by XRD (Bruker, D8 Advance) using a Cu K α monochrome target. The morphology of the alloy was examined by SEM (Shinadzu Corporation, SSX-550) at an accelerating voltage of 15 kV, and the micro-composition of the deposited alloy was measured using EDS coupled with SEM.

Results and Discussion

Electrochemical behavior of Dy(III) in eutectic NaCl-KCl on a tungsten electrode.—As described above, previous researches held different viewpoints concerning the electrochemical reduction mechanism of Dy(III). In this work, investigations on the electrochemical behavior of dysprosium stated with cyclic voltammograms (CVs) to further assess the nature of the employed system and the reversibility of the redox reaction. Figure 2 displays the representative CVs obtained on a tungsten electrode in the eutectic NaCl-KCl melts before and after the addition of 1.0 mol% DyCl_3 . The blue dotted line represents the typical CV curve for the blank NaCl-KCl melts. Only one cathodic signal A_c appears at about -2.14 V which is attributed to the deposition of sodium, and the corresponding anodic peak A_a in the reverse scan direction corresponds to the dissolution of the deposited sodium. No other additional redox signals are present in the line, confirming the applicability of the eutectic NaCl-KCl for the investigations.

The red solid line in Fig. 2 shows the CV with the addition of DyCl_3 . In the negative-going sweep, the cathodic current increases quickly from approximately -2.04 V , which is obviously steeper than that observed for the deposition of sodium metal. No alloy exists in the Dy-W or Dy-Na binary system,³⁹ and this current thus should be ascribed to the deposition of dysprosium metal.



During the positive scan, a new anodic peak B_a which is associated with the subsequent oxidation of Dy(0) to Dy(III), is observed. It can

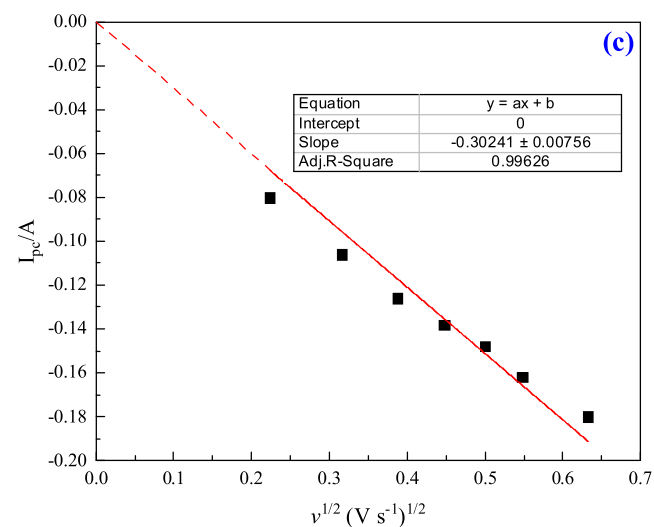
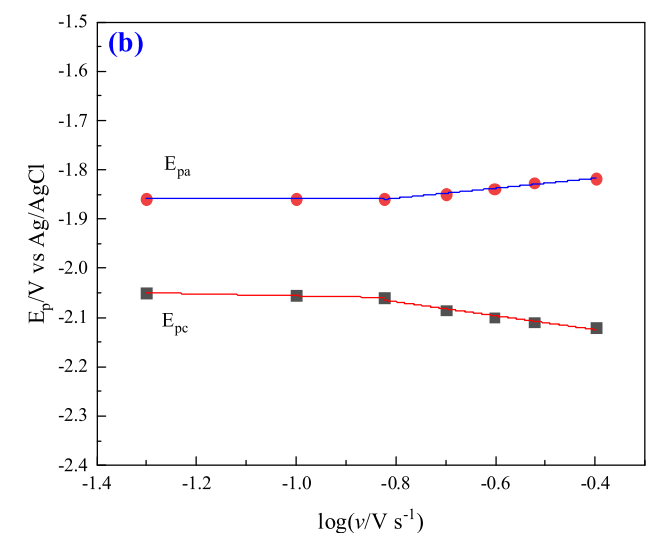
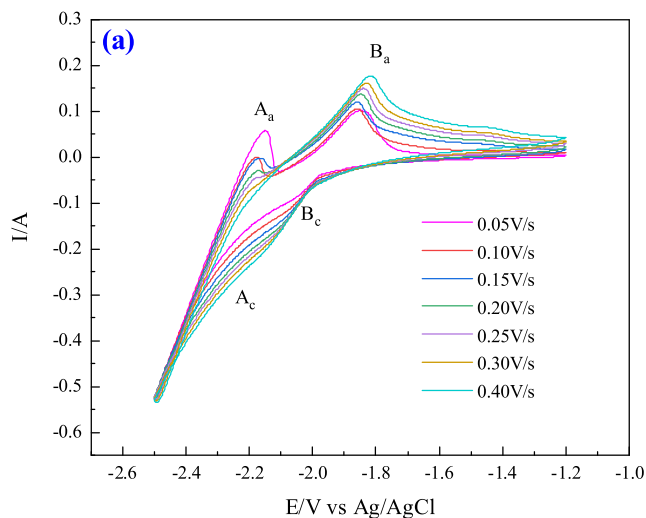


Figure 3. (a) CVs obtained in the NaCl-KCl-DyCl₃(1.0 mol%) melts at various scan rates (0.05~0.4 V s⁻¹) on a tungsten electrode ($S = 0.322 \text{ cm}^2$) at 700 °C; (b) Variation of the anodic and cathodic peak potentials with the logarithm of the scan rate at 700 °C; (c) Plot of the cathodic peak current as a function of the square root of the scan rate.

be seen that the cathodic signal B_c is not evident and overlaps with the signal A_c, because the deposition potential of dysprosium is very close to that of sodium. Similar phenomenon has also been reported

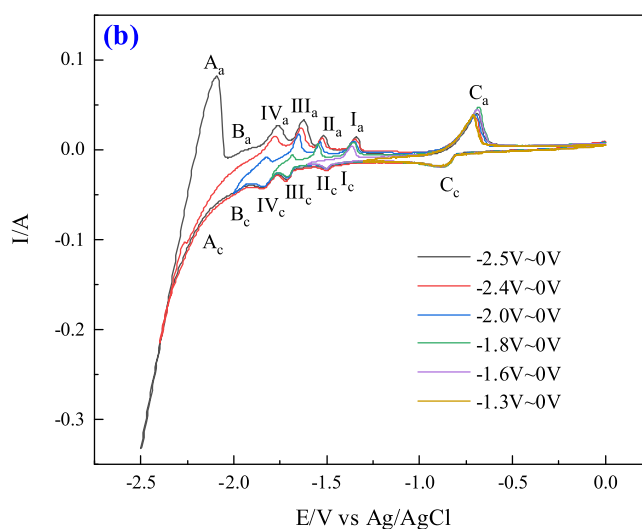
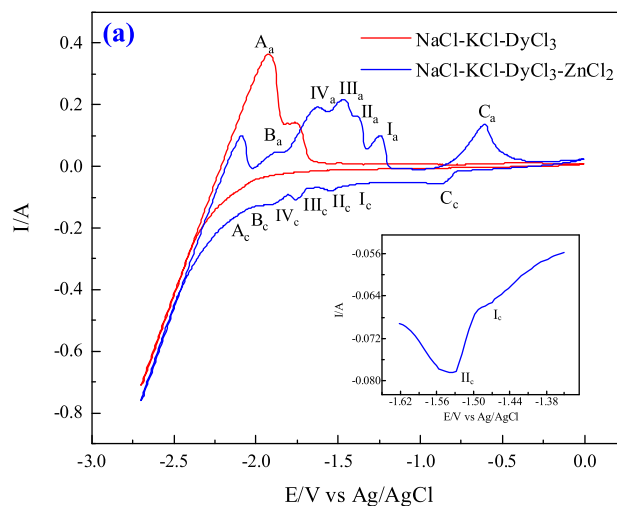


Figure 4. (a) CVs obtained in the NaCl-KCl-DyCl₃(1.0 mol%) melts (red line) and NaCl-KCl-DyCl₃(1.0 mol%)-ZnCl₂(1.0 mol%) melts (blue line) on a tungsten electrode ($S = 0.322 \text{ cm}^2$); (b) CVs of NaCl-KCl-DyCl₃(1.0 mol%)-ZnCl₂(1.0 mol%) melts measured on a tungsten electrode ($S = 0.322 \text{ cm}^2$) at different terminal potentials. Temperature: 700 °C, scan rate: 0.1 V s⁻¹.

by Yasuda et al. in the electrochemical fabrication of Dy-Ni alloys.³³ To further identify the reduction potential of dysprosium metal, the cathodic terminal potential was adjusted to -2.40 V. As shown by the inset in Fig. 2, in the blank NaCl-KCl melts, the anodic current is not very noticeable since only a small quantity of sodium deposits in the negative-going scan to -2.40 V. After the addition of DyCl₃, the cathodic current increases at around -2.04 V, and the oxidation peak shows a much higher amplitude in the reverse positive sweep. Therefore, it can be inferred that the unnoticeable cathodic signal B_c at approximately -2.04 V, whose potential is a little positive to the deposition potential of sodium, is related to the deposition of dysprosium metal. Except for the two signal couples A_a/A_a and B_c/B_a, no other redox signal is present in the CV curves for NaCl-KCl-DyCl₃ melts. It is probable that the deposition of dysprosium metal on a tungsten electrode in NaCl-KCl melts would be a one-step process by direct reduction of Dy(III) to Dy(0).

Furthermore, CVs on a tungsten electrode over a wide scan rate range from 0.05 to 0.40 V s⁻¹ were recorded to evaluate the reversibility of the redox reaction of Dy(III)/Dy(0) in NaCl-KCl-DyCl₃(1.0 mol%) melts, as shown in Fig. 3a. For a completely reversible electrode reaction, the ΔE_p ($\Delta E_p = |E_{pa} - E_{pc}|$) should have a constant value of $2.3RT/nF$ or 0.064 V for a three-electron reaction at 700 °C. It can be seen from Fig. 3b, the peak potentials almost remain stable and the value

of ΔE_p is nearly unchanged at low scan rates. But, the value of ΔE_p is found to exceed 0.064 V in this case. A similar behavior was also observed by Zhang et al. when they investigated the electrochemical behavior of Pb(II) in molten LiCl-KCl.⁴⁰ It is reported that the potential shift is probably correlated with the ohmic drop in the electrolytic cell and the experimental conditions.⁴¹ Whereas at higher scan rates, the cathodic and anodic peak potentials shift slightly toward negative and positive directions, respectively. Thus, the redox reaction of dysprosium on the inert tungsten electrode in the NaCl-KCl eutectic is considered to be quasi-reversible, but not fully reversible. In addition, the cathodic peak current (I_{pc}) of B_c increases as the scan rate increasing. The plot of the cathodic peak current vs the square root of the scan rate exhibits a good linear relationship in Fig. 3c, suggesting that electrochemical reduction of Dy(III) to Dy(0) in NaCl-KCl melts is a diffusion-controlled process. For a quasi-reversible soluble/insoluble system, the diffusion coefficient can be quantitatively determined by the Berzins—Delahay equation⁴²:

$$I_{pc} = -0.61SC_0(nF)^{3/2}D^{1/2}\nu^{1/2}(RT)^{-1/2} \quad [2]$$

where S denotes the electrode surface area (cm^2), C_0 is the solute concentration (mol cm^{-3}), n represents the number of electrons exchanged, F is the Faraday constant ($96,485 \text{ C mol}^{-1}$), D is the diffusion coefficient ($\text{cm}^2 \text{ s}^{-1}$), ν designates the potential scanning rate (V s^{-1}), R is the universal gas constant ($8.314 \text{ J mol}^{-1} \cdot \text{K}^{-1}$), and T corresponds to the absolute temperature (K). According to the slope of the fitting line in Fig. 3c, the diffusion coefficient of Dy(III) ions under this experimental conditions is calculated to be $1.7 \times 10^{-5} \text{ cm}^2 \text{ s}^{-1}$ by assuming that $n = 3$.

Electrochemical co-reduction of Dy(III) and Zn(II) in eutectic NaCl-KCl on tungsten electrode.—*Cyclic voltammetry.*—Figure 4a illustrates the comparison of CVs attained in NaCl-KCl-DyCl₃ (1.0 mol%) melts on tungsten electrode with and without ZnCl₂ addition. Except for the redox signals of A_c/A_a and B_c/B_a , corresponding to the deposition and subsequent dissolution of sodium and dysprosium metal, respectively, five new couples of redox signals are present in the CV curve after the addition of ZnCl₂ into the NaCl-KCl-DyCl₃ melts. The cathodic peak C_c and the corresponding anodic peak C_a at around $-0.8/-0.6 \text{ V}$ are attributed to the reduction/re-oxidation of liquid zinc metal. The redox potential of Zn(II)/Zn(0) closely approximates to that detected by Li et al.⁴³ The four couples of redox peaks, I_c/I_a , II_c/II_a , III_c/III_a and IV_c/IV_a located between the cathodic/anodic signals of B_c/B_a and C_c/C_a , should be ascribed to the deposition/dissolution of four different Dy-Zn intermetallic compounds. Obviously, compared with the deposition of pure dysprosium on inert tungsten electrode, co-reduction of Dy(III) with Zn(II) allows the deposition of dysprosium to occur at more positive potentials. Owing to the simultaneous deposition of zinc, the dysprosium metal deposits essentially on an active cathode of liquid zinc and alloys with zinc to form various Dy-Zn intermetallic compounds. These reduction peaks are very close and overlap each other because of their fairly similar deposition potentials. This phenomenon is similar to the underpotential deposition of dysprosium at active cathodes^{22,30,32–35,44} such as bismuth, aluminum, magnesium, nickel, and iron. The co-reduction process and formation mechanism of Dy-Zn alloy will be further discussed in the following section.

To assign the affiliation of these redox peaks, the CVs were subsequently measured at different terminal potentials in the same molten salt system. As shown in Fig. 4b, the cathodic peaks I_c , II_c , III_c and IV_c appear successively as the cathodic terminal of the potential selectively varying from -1.3 to -2.5 V . Strangely, the anodic peak II_a did not appear as the cathodic terminal potential was set at -1.6 V , and until the cathodic terminal potential reached to -1.8 V , the anodic peak II_a presented at around -1.5 V . This is probably because the amount of the deposited intermetallic compound related to the cathodic signal II_c is not sufficient when the cathodic terminal potential is not negative

enough, and thus resulting in the non-detectable anodic signal in subsequent positive scan. A similar behavior has also been detected by Tang et al.¹⁴ The values of redox peak potentials are presented in Table I. It is noteworthy that according to the Dy-Zn phase diagram, seven intermetallics could be formed at $700 \text{ }^\circ\text{C}$. However, only four couples of signals ascribed to Dy-Zn intermetallics were detected in the CV curves. The absence of the other three Dy-Zn intermetallics could be due to their similar deposition potentials to those of the detected signals, and the very slow formation of these compounds.³⁷

Square wave voltammetry.—Since the cathodic peaks I_c and II_c cannot be clearly confirmed by the CVs, square wave voltammetry, a more sensitive technique than cyclic voltammetry, was then conducted to further clarify reduction peak potentials of various Dy-Zn intermetallics and to explore the electrochemical co-reduction process of Dy (III) and Zn (II). Figure 5 presents the square wave voltammogram (SWV) measured on a tungsten electrode in NaCl-KCl-DyCl₃(1.0 mol%)-ZnCl₂(1.0 mol%) melts at a step potential of 1 mV and frequency of 100 Hz at $700 \text{ }^\circ\text{C}$. Seven obvious peaks can be clearly distinguished from Fig. 5. It is evident that the peaks A_c , B_c and C_c are attributed to the reduction reactions of Na(I), Dy(III) and Zn(II) to their pure metals, respectively. The other four reduction peaks, from I_c to IV_c , are associated with the formation of various Dy-Zn intermetallic compounds. Moreover, the reduction peak I_c is very close to the peak II_c . The above results are in good agreement with those from CVs in Fig. 4. The reduction potentials of these seven peaks detected by SWV are also listed in Table I, convincingly confirming the potential values for the formation of different Dy-Zn intermetallic compounds observed in CVs.

Open circuit chronopotentiometry.—Open circuit chronopotentiometry is an appropriate electrochemical technique for the research of underlying alloy formation and dissolution process. In this method, potentiostatic electrolysis at -2.40 V was firstly carried out in the NaCl-KCl-DyCl₃(1.0 mol%)-ZnCl₂(1.0 mol%) melts for 60 s to form a thin layer specimen on the tungsten electrode, and then the open circuit potential of the electrode was recorded vs time. The interaction and diffusion between the deposited dysprosium and zinc metals results in the formation of various Dy-Zn phases, and meanwhile, the electrode potential gradually shifts towards positive. During this process, successive potential plateaus can be observed, and each plateau signifies an electrochemical equilibrium within the range of two phases coexisting state.^{45,46}

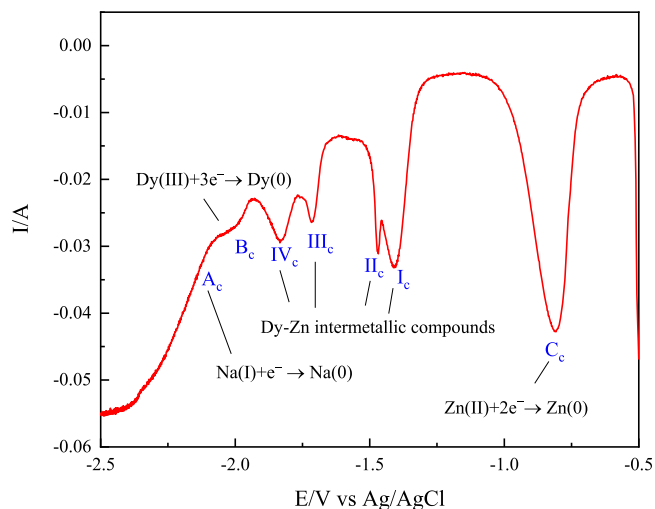


Figure 5. SWV attained in the NaCl-KCl-DyCl₃(1.0 mol%)-ZnCl₂(1.0 mol%) melts on a tungsten electrode ($S = 0.322 \text{ cm}^2$) at $700 \text{ }^\circ\text{C}$. Potential step: 1 mV, frequency: 100 Hz.

Table I. Summary of the results obtained by cyclic voltammetry, square wave voltammetry, open circuit chronopotentiometry techniques in molten NaCl-KCl-DyCl₃(1.0 mol%)-ZnCl₂(1.0 mol%) on a tungsten electrode at 700 °C.

Peak	A	B	IV	III	II	I	C
Reduction/oxidation peak potential in CV (V)	-2.14/-2.10	-2.01/-1.93	-1.83/-1.76	-1.71/-1.62	-1.52/-1.49	-1.42/-1.32	-0.86/-0.69
Reduction peak potential in SWV (V)	-2.12	-2.00	-1.83	-1.71	-1.47	-1.40	-0.81
Oxidation peak potential in OCP (V)	-2.02	-1.94	-1.82	-1.68	-1.57	-1.39	-0.85

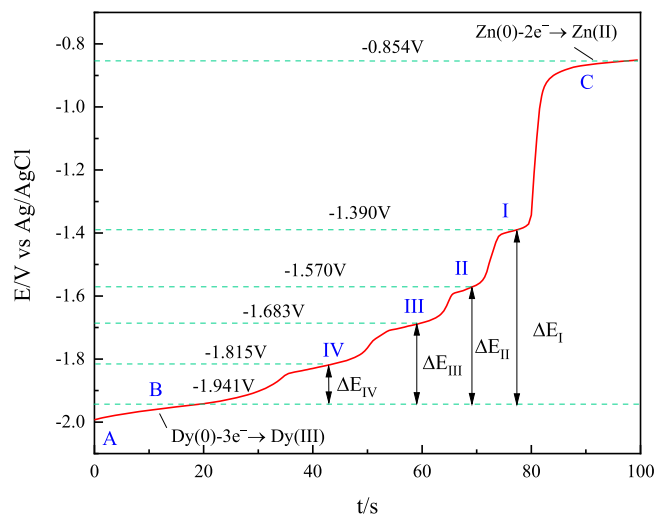
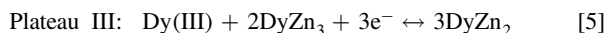
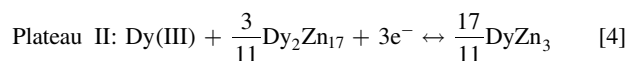
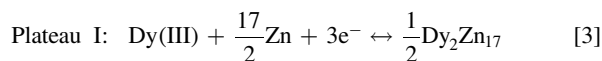


Figure 6. Open circuit potential transient curve recorded on a tungsten electrode ($S = 0.322 \text{ cm}^2$) after electrodepositing at -2.4 V vs Ag/AgCl for 60 s in $\text{NaCl-KCl-DyCl}_3(1.0 \text{ mol}\%)\text{-ZnCl}_2(1.0 \text{ mol}\%)$ melts at 700°C .

The open circuit chronopotentiogram (OCP) of $\text{NaCl-KCl-DyCl}_3(1.0 \text{ mol}\%)\text{-ZnCl}_2(1.0 \text{ mol}\%)$ melts on a tungsten electrode is illustrated in Fig. 6, and seven plateaus can be clearly seen. The plateau potentials, representing the two-phase coexisting state, are also presented in Table I. In the beginning, the potential staying at around -2.02 V (plateau A), is attributed to the re-oxidation of the deposited sodium metal on tungsten electrode and corresponds to the $\text{Na(I)}/\text{Na(0)}$ redox couple. Afterward, plateau B at -1.94 V is correlated with the $\text{Dy(III)}/\text{Dy(0)}$ system. The last plateau (plateau C) appearing at approximately -0.85 V should be ascribed to $\text{Zn(II)}/\text{Zn(0)}$ redox couple. Apart from these three potential plateaus, the chronopotentiogram also exhibits four plateaus I, II, III and IV, which is considered to be caused by the dissolution of different Dy-Zn intermetallic compounds. The closer the equilibrium potential of the phase to that of Dy metal, the higher Dy content could be formed in the Dy_xZn_y phase.²⁶ According to the following XRD and SEM-EDS analyses, the plateaus I, II, III and IV in Fig. 6 could be ascribed to the following equilibrium reactions, respectively:



Thermodynamic properties of Dy-Zn intermetallic compounds.—Compared with the transient electrochemical techniques such as

cyclic voltammetry and square wave voltammetry, open circuit chronopotentiometry, which is immune to the nucleation overpotential, is more suitable to determine the equilibrium potential of the redox system,⁴³ and electromotive force measurement can then be performed to investigate the thermodynamic formation of the intermetallic compounds. Based on the results of OCP from Fig. 6, the equilibrium potentials of different Dy-Zn intermetallics prepared by electrochemical co-reduction of Dy(III) and Zn(II) , referencing to the Ag/AgCl couple, could be converted to the electromotive force against Dy(0) . The electromotive force, corresponding to the chemical composition of the intermetallic compound, is in connection with the activity and the relative partial molar Gibbs energy of dysprosium, as expressed as follows:

$$\Delta\bar{G}_{\text{Dy}} = -3F\Delta E = RT \ln(a_{\text{Dy}}(\text{in } \text{Dy}_x\text{Zn}_y)) \quad [7]$$

where $\Delta\bar{G}_{\text{Dy}}$ represents the relative partial molar Gibbs energy of dysprosium in the Dy_xZn_y intermetallic compound ($\text{kJ}(\text{mol Dy})^{-1}$), ΔE denotes potential (V) of Dy_xZn_y intermetallic compound referencing to the $\text{Dy(III)}/\text{Dy(0)}$, and a_{Dy} (in Dy_xZn_y) is the activity of dysprosium in the Dy_xZn_y intermetallic compound, choosing pure dysprosium as the standard state. Subsequently, the two thermodynamic properties of various Dy-Zn intermetallic compounds can be estimated, as listed in Table II. It can be seen that the activities of dysprosium in the two-phase coexisting state are in the order of 10^{-9} to 10^{-2} . Moreover, the value of dysprosium activity in Dy-Zn becomes smaller when zinc is more prevalent in the two-phase coexisting state. For example, activity of dysprosium in the two-phase state of $\text{Zn-Dy}_2\text{Zn}_{17}$ is in the order of 10^{-9} , while it is in the order of 10^{-2} in the $\text{DyZn}_2\text{-DyZn}$ coexisting phase. This result will offer an insight into controlling an appropriate rate and time of the electrorefining technology for the spent nuclear fuel processing.

In addition, according to the equilibrium reactions, the standard molar Gibbs free energies of formation for various Dy-Zn intermetallic compounds at 700°C are calculated and the obtained values are presented in Table III.

Dy-Zn alloy formation mechanism via electrochemical co-reduction.—The electrochemical co-reduction usually refers to the simultaneous reduction of two or more metallic ions to form alloys on an inert electrode. It has exhibited more benefits for alloy preparation in terms of homogeneity of alloy composition, feasibility of continuous process and cost saving.^{29,47} Consequently, the co-reduction approach has been introduced in molten salt system for spent nuclear fuel reprocessing.

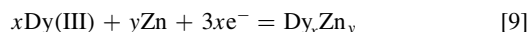
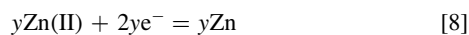
According to the results from CV, SWV and OCP, Dy(III) in molten chlorides could be reduced with Zn(II) on an inert electrode to form Dy-Zn alloy, although the redox potential of $\text{Dy(III)}/\text{Dy(0)}$ is more negative than that of $\text{Zn(II)}/\text{Zn(0)}$. In fact, the so-called co-reduction does not refer to the simultaneous reduction of various metallic ions at the same potential. In the case of two metallic ions in this work, Zn(II) in eutectic NaCl-KCl melts is preferentially reduced and form a liquid zinc film on the inert tungsten electrode, and Dy(III) is subsequently reduced on the zinc-coated electrode and reacts with zinc to generate various Dy-Zn intermetallic compounds. Hence, the electrochemical formation of Dy-Zn alloy is considered to include the two consecutive steps described as follows:

Table II. Thermodynamic properties of Dy in the two-phase coexisting states

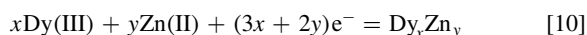
Plateau	E/V (vs Ag/AgCl)	E/V (vs Dy(III)/Dy(0))	$\Delta\bar{G}_{\text{Dy}}/(\text{kJ}\cdot(\text{mol Dy})^{-1})$	a_{Dy}
B	-1.941 ± 0.002			
IV	-1.815 ± 0.001	0.126 ± 0.003	-36.47 ± 0.87	1.10×10^{-2}
III	-1.683 ± 0.003	0.258 ± 0.005	-74.68 ± 1.45	9.79×10^{-5}
II	-1.570 ± 0.003	0.371 ± 0.005	-107.39 ± 1.45	1.72×10^{-6}
I	-1.390 ± 0.004	0.551 ± 0.006	-159.49 ± 1.74	2.74×10^{-9}

Table III. The calculation formula and standard molar Gibbs free energies of formation for various Dy-Zn intermetallic compounds.

Intermetallic compounds	Equation	$\Delta G_f^\theta / (\text{kJ} \cdot \text{mol}^{-1})$
$\text{Dy}_2\text{Zn}_{17}$	$\Delta G_f^\theta(\text{Dy}_2\text{Zn}_{17}) = -3F\Delta E_{\text{I}}$	-159.49 ± 1.74
DyZn_3	$\Delta G_f^\theta(\text{DyZn}_3) = 11/17[3/11\Delta G_f^\theta(\text{Dy}_2\text{Zn}_{17}) - 3F\Delta E_{\text{II}}]$	-97.63 ± 1.24
DyZn_2	$\Delta G_f^\theta(\text{DyZn}_2) = 1/3[2\Delta G_f^\theta(\text{DyZn}_3) - 3F\Delta E_{\text{III}}]$	-89.98 ± 1.31
DyZn	$\Delta G_f^\theta(\text{DyZn}) = 1/2[\Delta G_f^\theta(\text{DyZn}_2) - 3F\Delta E_{\text{IV}}]$	-63.23 ± 1.09



The overall process of the formation of Dy-Zn alloy can be written as follows:



The equilibrium potential of the system $\text{Dy(III)}/\text{Dy}_x\text{Zn}_y$ can be expressed as:

$$\begin{aligned} E_{\text{Dy(III)}/\text{Dy}_x\text{Zn}_y} &= E_{\text{Dy(III)}/\text{Dy(0)}}^0 + \frac{RT}{nF} \ln \left[\frac{a_{\text{Dy(III)}}}{a_{\text{Dy}}(\text{in } \text{Dy}_x\text{Zn}_y)} \right] \\ &= E_{\text{Dy(III)}/\text{Dy(0)}}^{\text{equ}} - \frac{RT}{nF} \ln a_{\text{Dy}}(\text{in } \text{Dy}_x\text{Zn}_y) \end{aligned} \quad [11]$$

where $E_{\text{Dy(III)}/\text{Dy(0)}}^0$ and $E_{\text{Dy(III)}/\text{Dy(0)}}^{\text{equ}}$ represents the standard redox potential and the equilibrium potential of pure dysprosium (V), respectively, $a_{\text{Dy(III)}}$ and $a_{\text{Dy}}(\text{in } \text{Dy}_x\text{Zn}_y)$ are the activities of the Dy(III) and Dy(0) in Dy-Zn intermetallic compound, respectively.

Since the activity of dysprosium in Dy-Zn intermetallic is less than unity, the relation $E_{\text{Dy(III)}/\text{Dy}_x\text{Zn}_y} > E_{\text{Dy(III)}/\text{Dy(0)}}^{\text{equ}}$ is evident, according to the Nernst equation. Consequently, the equilibrium redox potential of Dy(III)/Dy(0) system shifts more positive. This explains why the co-reduction of Dy(III) and Zn(II) to form their alloy can make the deposition of dysprosium occur at more positive potentials. Moreover, the activities of dysprosium in various Dy-Zn intermetallic compounds present different values, and thus the four reduction signals corresponding to the formation of four different Dy-Zn intermetallic compounds are present in the CVs and SWV, as shown in Figs. 4 and 5, respectively.

Potentiostatic electrolysis and characterization of Dy-Zn alloy.—Based on the results from cyclic voltammetry, square wave voltammetry and open circuit chronopotentiometry, potentiostatic electrolysis was carried out at -2.0 V on a tungsten electrode for 11 h, to examine the formation of Dy-Zn alloy via co-reduction of Dy(III) and Zn(II) from NaCl-KCl melts at 700 °C. Figure 7 displays the evolution of the cathodic current vs time during electrolysis. In the initial stage, the current keeps increasing and rises up to approximately -0.7 A in a short period of 3800 s because the surface area of the cathode is continually enlarged with the deposition of Dy-Zn alloys. Afterward, the current maintains around -0.7 A for about 2700 s. This is likely attributed to the balance of the contribution from surface enlargement and the ions depletion of Dy(III) and Zn(II) in the melts. After continuous electrolysis for about 6500 s, the tungsten cathode is probably covered by a thick layer of Dy-Zn alloy. According to the Dy-Zn binary phase diagram, all the Dy-Zn intermetallic compounds are in solid state at 700 °C. Therefore, Dy-Zn alloy powders (see inset photo in Fig. 7) should deposit on the cathode. Due to the weak adhesive force of the fine Dy-Zn powders, they cannot attach to cathode and incessantly fall off from the cathode. Consequently, the surface area is reducing, resulting in the continual decrease of the current. When an

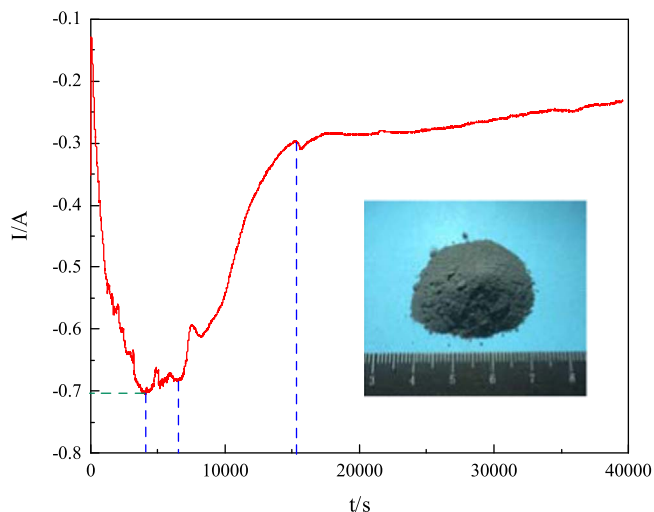


Figure 7. Typical evolution of cathodic current during potentiostatic electrolysis obtained on a tungsten electrode ($S = 0.761 \text{ cm}^2$) in molten NaCl-KCl-DyCl₃(1.0 mol%)-ZnCl₂(1.0 mol%) at 700 °C. Inset photo: Dy-Zn alloy powders obtained by potentiostatic electrolysis.

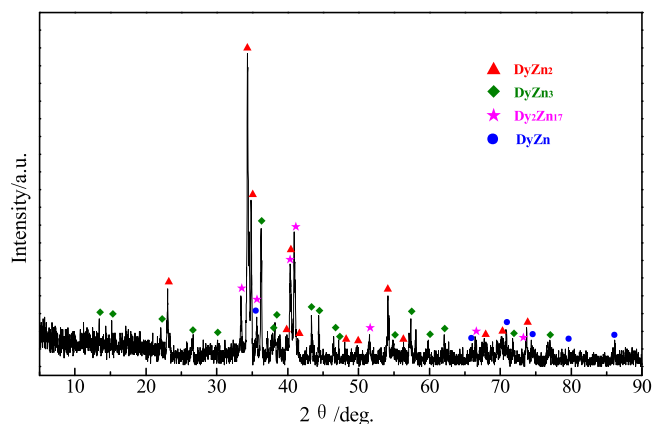


Figure 8. XRD pattern of the deposits obtained by potentiostatic electrolysis at -2.0 V for 11 h on tungsten electrode in molten NaCl-KCl-DyCl₃(1.0 mol%)-ZnCl₂(1.0 mol%) at 700 °C.

electrolysis time of 15000 s is reached, the electrolysis progresses into the final stage, and the current is tardily decreasing because of the serious depletion of Dy(III) and Zn(II) ions in the melts after long time electrolysis. Meanwhile, it is clear to note that some small sudden fluctuation occurs occasionally, which can be attributed to the variation of the electrode surface by the fall-off of powdery deposits.

Figure 8 shows the XRD pattern of the deposits obtained by potentiostatic electrolysis at -2.0 V for 11 h in molten NaCl-KCl-DyCl₃(1.0 mol%)-ZnCl₂(1.0 mol%) at 700 °C. The observed peaks in the patterns are identified as DyZn₂, Dy₂Zn₁₇,

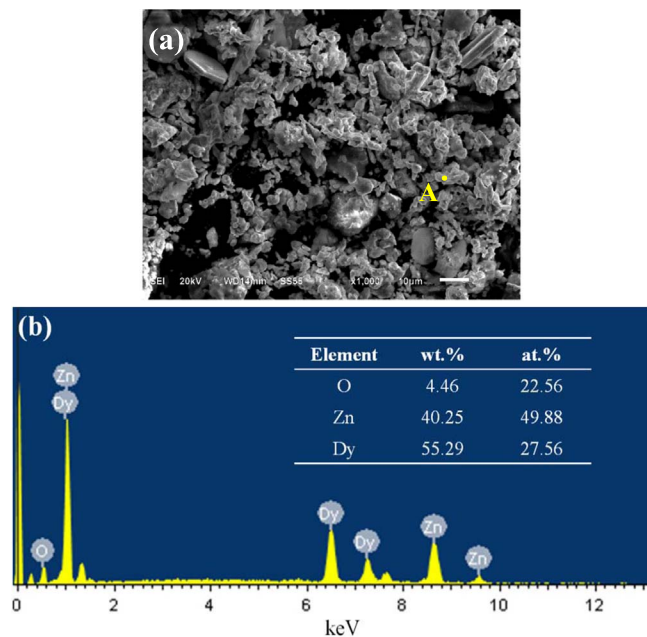


Figure 9. SEM image (a) and EDS analysis (b) of the deposits obtained by potentiostatic electrolysis at -2.0 V for 11 h on tungsten electrode in molten NaCl-KCl-DyCl₃(1.0 mol%)-ZnCl₂(1.0 mol%) at 700 °C.

DyZn₃ and DyZn, in agreement with the results observed in CVs, SWV and OCP. The intermetallic compound DyZn₃ has also been detected in the products obtained by potentiostatic electrolysis in molten LiCl-KCl-DyCl₃ on a zinc wire.⁴⁸ Meanwhile, it can be seen that the alloy sample is mainly composed of DyZn₂. This is perhaps ascribed to the relatively low current density applied during electrolysis. The formation of other intermetallic compounds, of course, including Dy₂Zn₁₇, DyZn₃ and DyZn, would be kinetically slow, and transform to the thermodynamically more stable phases of DyZn₂. Similar phenomena have also been reported in electrochemical formation of Mg-Nd and Dy-Ni alloys in molten salts.^{36,37}

The surface microtopography and microzone composition of the deposits were further examined using SEM equipped with EDS quantitative analysis. Figure 9a is the SEM image of Dy-Zn alloy obtained by potentiostatic electrolysis at -2.0 V for 11 h. The deposition products are powders in irregular shape, with a diameter ranging from 2 μ m to 10 μ m. It is reasonable to infer that solid Dy-Zn alloy generates during electrolysis via the underpotential reduction of Dy(III) on pre-deposited zinc. The result of EDS analysis of the point marked A, as shown in Fig. 9b, indicates that the deposits are composed of elements of Zn, Dy and O. The presence of oxygen is presumably caused by oxidation because the fine powders of Dy-Zn alloy are easily oxidized. Moreover, the atom ratio Dy:Zn is close to 1:2, suggesting that the alloy obtained by potentiostatic electrolysis is mainly composed of the DyZn₂ intermetallic compound.

Conclusions

The electrochemical behavior of Dy(III) and its co-reduction process with Zn(II) on an inert tungsten electrode was investigated in eutectic NaCl-KCl melts containing 1.0 mol% DyCl₃ and 1.0 mol% ZnCl₂ at 700 °C by various electrochemical techniques. The results of CVs indicate that the Dy(III) ions are directly reduced to Dy(0) on a tungsten electrode through a single step with three electrons exchanged. The reduction process is found to be quasi-reversible and controlled by the diffusion of Dy(III) ions in melts with the diffusion coefficient estimated to be approximately 1.7×10^{-5} cm² s⁻¹.

The results of CVs and SWV and OCP measured in the NaCl-KCl-DyCl₃-ZnCl₂ show that the underpotential deposition of dysprosium occurs on the pre-reduced zinc metal due to the formation of various Dy-Zn intermetallic compounds. The

electromotive force measurements for Dy-Zn intermetallic compounds in two-phase coexisting state were performed. Based on the results of electromotive force measurements, the thermodynamic properties including the activities and relative partial molar Gibbs energies of dysprosium in the Dy-Zn alloy, and the formation Gibbs energies for four Dy-Zn intermetallic compounds, were determined.

Electrochemical deposition of Dy-Zn alloy was carried out by potentiostatic electrolysis at -2.0 V for 11 h on a tungsten electrode in NaCl-KCl-DyCl₃(1.0 mol%)-ZnCl₂(1.0 mol%) melts at 700 °C. During electrolysis, solid Dy-Zn alloy should generate on the tungsten electrode via the underpotential reduction of Dy(III) on the pre-deposited zinc. The obtained powdery Dy-Zn alloy mainly consists of DyZn₂, with the intermetallic compounds of DyZn₃, DyZn and Dy₂Zn₁₇ as the minor phase composition. The extraction of dysprosium by electrochemical deposition with zinc from molten NaCl-KCl-DyCl₃-ZnCl₂ on an inert electrode at 700 °C was proved to be practically feasible, and provided a theoretical reference for the future reprocessing of spent nuclear fuel based on pyrochemical electrorefining process.

Acknowledgments

This work was financially supported by the Anhui Provincial Natural Science Foundation (2008085ME170), the National Natural Science Foundation of China (51204002 and 51904003), the Developing Program Foundation for the Excellent Youth Talents of Higher Education of Anhui Province (gxyq2018012) and the Foundation of Anhui Province Key Laboratory of Metallurgical Engineering & Resources Recycling (SKF19-05). The authors are particularly grateful to Professor Dongming Liu for the kind help on XRD analysis.

ORCID

Zhongsheng Hua  <https://orcid.org/0000-0002-5984-1336>

References

1. Y. Yan, X. Li, M. Zhang, Y. Xue, H. Tang, W. Han, and Z. Zhang, *J. Electrochem. Soc.*, **159**, D649 (2012).
2. P. Souček, R. Malmbeck, E. Mendes, C. Nourry, D. Sedmidubský, and J. P. Glatz, *J. Nucl. Mat.*, **394**, 26 (2009).
3. J. Cetnar, G. Domańska, P. Gajda, and J. Janczyszyn, *Nukleonika*, **59**, 137 (2014).
4. W. Duan, C. Xu, J. Wang, S. Wang, J. Wang, and J. Chen, *Sep. Sci. Technol.*, **50**, 1249 (2015).
5. K. Kinoshita, T. Inoue, S. Fusselman, D. Grimmett, J. Roy, R. Gay, C. Krueger, C. Nabelek, and T. Storvick, *J. Nucl. Sci. Technol.*, **36**, 189 (1999).
6. C. Nourry, L. Massot, P. Chamelot, and P. Taxil, *J. Appl. Electrochem.*, **39**, 927 (2009).
7. M. Salvatore and G. Palmiotti, *Prog. Part. Nucl. Phys.*, **66**, 144 (2011).
8. M. Gibilaro, L. Massot, P. Chamelot, and P. Taxil, *J. Nucl. Mat.*, **382**, 39 (2008).
9. P. Taxil, L. Massot, C. Nourry, M. Gibilaro, P. Chamelot, and L. Cassayre, *J. Fluorine Chem.*, **130**, 94 (2009).
10. K. C. Marsden and B. Pesic, *J. Electrochem. Soc.*, **158**, F111 (2011).
11. Y. Sakamura, O. Shirai, T. Iwai, and Y. Suzuki, *J. Alloy. Compd.*, **321**, 76 (2001).
12. M. Iizuka, K. Uozumi, T. Inoue, T. Iwai, O. Shirai, and Y. Arai, *J. Nucl. Mat.*, **299**, 32 (2001).
13. K. Uozumi, M. Iizuka, T. Kato, T. Inoue, O. Shirai, T. Iwai, and Y. Arai, *J. Nucl. Mat.*, **325**, 34 (2004).
14. H. Tang, Y. Yan, M. Zhang, X. Li, Y. Huang, Y. Xu, Y. Xue, W. Han, and Z. Zhang, *Electrochim. Acta*, **88**, 457 (2013).
15. O. Shirai, M. Iizuka, T. Iwai, and Y. Arai, *Anal. Sci.*, **17**, 51 (2001).
16. L. Rault, M. Heusch, M. Allibert, F. Lemort, X. Deschanel, and R. Boen, *Nucl. Technol.*, **139**, 167 (2002).
17. O. Conocar, N. Douyere, J. P. Glatz, J. Lacquement, R. Malmbeck, and J. Serp, *Nucl. Sci. Eng.*, **153**, 253 (2006).
18. J. Serp, M. Allibert, A. L. Terrier, R. Malmbeck, M. Ougier, J. Rebizant, and J. P. Glatz, *J. Electrochem. Soc.*, **152**, C167 (2005).
19. L. Cassayre, R. Malmbeck, P. Massot, J. Rebizant, J. Serp, P. Soucek, and J. P. Glatz, *J. Nucl. Mat.*, **360**, 49 (2007).
20. M. Gibilaro, L. Massot, P. Chamelot, and P. Taxil, *Electrochim. Acta*, **54**, 5300 (2009).
21. D. Hudry, I. Bardes, A. Rakhnatullin, C. Bessada, F. Bart, S. Jobic, and P. Deniard, *J. Nucl. Mat.*, **381**, 284 (2008).
22. S. Wang, B. Wei, M. Li, W. Han, M. Zhang, X. Yang, and Y. Sun, *J. Rare Earths*, **36**, 1007 (2018).
23. K. Chang, X. Lu, F. Du, and M. Zhao, *Chinese J. Chem.*, **12**, 509 (1994).
24. H. Konishi, T. Nohira, and Y. Ito, *Electrochem. Solid ST.*, **5**, B37 (2002).

25. M. Zhang, Y. Yang, W. Han, M. Li, K. Ye, Y. Sun, and Y. Yan, *J. Solid State Electr.*, **17**, 2671 (2013).
26. L. Su, K. Liu, Y. Liu, L. Wang, L. Yuan, L. Wang, Z. Li, X. Zhao, Z. Chai, and W. Shi, *Electrochim. Acta*, **147**, 87 (2014).
27. H. B. Kushkhov, A. S. Uzdanova, M. M. A. Saleh, A. M. F. Qahtan, and L. A. Uzdanova, *Am. J. Anal. Chem.*, **4**, 39 (2013).
28. C. Hamel, P. Chamelot, and P. Taxil, *Electrochim. Acta*, **49**, 4467 (2004).
29. Y. Shi, X. Liu, Y. Gao, C. Huang, and B. Li, *J. Electrochem. Soc.*, **164**, D263 (2017).
30. Y. Castrillejo, M. Bermejo, A. Barrado, R. Pardo, E. Barrado, and A. Martínez, *Electrochim. Acta*, **50**, 2047 (2005).
31. Y. Liu, G. Liu, and Q. Yang, "Electrochemical behaviors of Dy(III) in fluoride melts." *Journal of Inner Mongolia University of Technology*, **11**, 57 (1992), (In Chinese).
32. Y. Yang et al., *Electrochim. Acta*, **118**, 150 (2014).
33. K. Yasuda, S. Kobayashi, T. Nohira, and R. Hagiwara, *Electrochim. Acta*, **106**, 293 (2013).
34. A. Saïla, M. Gibilaro, L. Massot, P. Chamelot, P. Taxil, and A. M. Affoune, *J. Electroanal. Chem.*, **642**, 150 (2010).
35. H. Konishi, T. Nohira, and Y. Ito, *Electrochim. Acta*, **47**, 3533 (2002).
36. S. Kobayashi, T. Nohira, K. Kobayashi, K. Yasuda, R. Hagiwara, T. Oishi, and H. Konishi, *J. Electrochem. Soc.*, **159**, E193 (2012).
37. Z. Hua, H. Liu, J. Wang, J. He, S. Xiao, Y. Xiao, and Y. Yang, *ACS Sustain. Chem. Eng.*, **5**, 8089 (2017).
38. J. He, Z. Hua, H. Liu, L. Xu, S. He, Y. Yang, and Z. Zhao, *J. Electrochem. Soc.*, **165**, E598 (2018).
39. T. B. Massalski, *Binary Alloy Phase Diagrams* (ASM International, Materials Park, OH) 2nd ed. (1996).
40. M. Zhang, L. Chen, W. Han, Y. Yan, and P. Cao, *Trans. Nonferrous Met. Soc. China*, **22**, 711 (2012).
41. Y. Castrillejo, M. R. Bermejo, P. Díaz Arocas, A. M. Martínez, and E. Barrado, *J. Electroanal. Chem.*, **575**, 61 (2005).
42. T. Berzins and P. Delahay, "Oscillographic polarographic waves for the reversible deposition of metals on solid electrodes." *J. Am. Chem. Soc.*, **75**, 5559 (1953).
43. M. Li, J. Wang, W. Han, X. Yang, M. Zhang, Y. Sun, M. Zhang, and Y. Yan, *Electrochim. Acta*, **228**, 299 (2017).
44. M. Li, T. Sun, B. Liu, W. Han, Y. Sun, and M. Zhang, *Acta Phys.-Chim. Sin.*, **31**, 309 (2015).
45. C. Nourry, L. Massot, P. Chamelot, and P. Taxil, "Formation of Ni-Nd alloys by Nd (III) Electrochemical Reduction in Molten Fluoride." *Journal of New Materials for Electrochemical Systems*, **10**, 117 (2007), https://www.researchgate.net/publication/27812857_Formation_of_NiNd_alloys_by_NdIII_electrochemicalreduction_in_molten_fluoride.
46. Y. Castrillejo, P. Fernandez, J. Medina, M. Vega, and E. Barrado, *Electroanal.*, **23**, 222 (2011).
47. S. Wei, M. Zhang, W. Han, Y. Yan, M. Zhang, and B. Zhang, *T. Nonferr. Metal. Soci. China*, **21**, 825 (2011).
48. H. Konishi, H. Ono, E. Takeuchi, T. Nohira, and T. Oishi, *ECS Trans.*, **61**, 19 (2014).